

Article

Acetonitrile's Effect on the Efficiency of Ethanol Electrooxidation at a Polycrystalline Pt Electrode in Relation to pH-Dependent Fuel Cell Applications

Bogusław Pierozynski ^{1,*}, Tomasz Mikołajczyk ^{1,*} , Mateusz Łuba ¹ , Paweł Wojtacha ²  and Lech Smoczyński ¹ 

¹ Department of Chemistry, Faculty of Environmental Management and Agriculture, University of Warmia and Mazury in Olsztyn, Łódzki Square 4, 10-727 Olsztyn, Poland; mateusz.luba@uwm.edu.pl (M.Ł.); lechs@uwm.edu.pl (L.S.)

² Department of Industrial and Food Microbiology, Faculty of Food Science, University of Warmia and Mazury in Olsztyn, Cieszyński Square 1, 10-726 Olsztyn, Poland; pawel.wojtacha@uwm.edu.pl

* Correspondence: bogpierzynski@yahoo.ca (B.P.); tomasz.mikolajczyk@uwm.edu.pl (T.M.); Tel.: +48-89-523-4177 (B.P.)

Received: 3 October 2020; Accepted: 3 November 2020; Published: 5 November 2020



Abstract: The present paper reports cyclic voltammetric and a.c. impedance spectroscopy investigations on the influence of the acetonitrile concentration on the kinetics (and individual product's efficiency) of the ethanol oxidation reaction (EOR), performed on a polycrystalline Pt electrode surface in 0.5 M H₂SO₄ and 0.1 M NaOH supporting solutions. The kinetics of the EOR were examined at room temperature over the voltammetric potential range, which covers the electrooxidation of surface-adsorbed CO_{Ads} species, as well as the formation of acetaldehyde molecules. In addition, the time-dependent efficiency of acetate and acetaldehyde formation in relation to the initial acetonitrile content for both acidic and alkaline electrolytes was evaluated by means of spectrophotometric Ultraviolet/Visible Spectroscopy (UV-VIS) instrumental analysis.

Keywords: ethanol electrooxidation; AcN; acetonitrile; poly Pt electrode; impedance spectroscopy

1. Introduction

The process of the electrochemical oxidation of alcohols has a direct application in the so-called Direct Alcohol Fuel Cells (DAFCs). As ultra-pure hydrogen fuel allows significantly greater electric efficiencies to be reached than aliphatic alcohols in a Proton Exchange Membrane (PEM) fuel cell, H₂ production, storage, and large-scale distribution still constitute significant technical problems. Conversely, the use of alcohols as hydrogen carriers in a DAFC device is beneficial, as liquid alcohol involves simplified fuel storage and distribution systems. In fact, methanol and ethanol are the most frequently investigated alcohols for PEM fuel cell applications, where C₂H₅OH is regarded as a promising substitute for CH₃OH, due to its considerably higher (8.0 vs. 6.1 kWh kg⁻¹) energy-density and the relatively low toxic properties of ethanol oxidation by-products (acetaldehyde and acetic acid). In addition, it has to be stressed that ethanol is a renewable resource as it can be produced from a variety of available agricultural-based products and biomass substrates [1–11].

The process of ethanol electrooxidation on platinum-based catalyst surfaces (the most important catalyst known in electrochemistry) is a complex anodic reaction, involving the formation of various, surface-adsorbed intermediates. It is commonly accepted [2,11–13] that following the surface electrosorption step, the C₂H₅OH molecule can either dissociate to surface-adsorbed CO_{Ads} species, or become electrooxidized to form acetaldehyde. Afterwards, in the presence of adsorbed hydroxyl groups, successive oxidation steps lead to the formation of carbon dioxide or acetic acid molecules,

which eventually become desorbed from the catalyst surface. A number of various catalyst materials have been extensively studied (both in acidic and alkaline media) in relation to the ethanol electrooxidation reaction. These include bulk polycrystalline and single-crystal planes of Pt [3,9,13–17], PtRu [2,18–20], PtRh [2,12,19,20], PtSn [1,2,6,7,15,21], PtPd [8,9], and many other alloys/co-deposits of Pd₂Sn [22], Pd₂Ru/C [23], or metal oxides [10,11] (typically on carbon substrates). In fact, Pt-PbO_x and Pd-CeO₂ binary nanocomposite systems were found [11] to be two of the most efficient ethanol oxidation reaction (EOR) catalysts with respect to their C-C bond cleavage capabilities. On the other hand, the electrooxidation of CO species adsorbed on the electrode surface was found to occur at lower potentials on catalysts containing Sn and SnO₂ additives when compared to single platinum group metals (e.g., Pd, Pt, and Rh) and their binary composites (e.g., Pt-Rh/C and Pd₂Ru/C) [23,24].

Moreover, the development of similar noble metal-based catalysts has been accelerated due to their high electrochemical activity in oxidation reactions of various organic compounds and the oxygen evolution reaction (OER), in relation to water electrolysis processes. The above is dictated by the development of global trends in environmental protection concentrated on the reduction of anthropological pollutants. Modern works on this topic include articles on carbon-supported Pt- and Pd-nanoparticle catalysts, e.g., Ru_{0.9}Pt_{0.1}O₂/C, Pt/C-LiCoO₂, and PtIr₂ alloy/C [25–28]. An advantage of such systems over bulk-type catalysts is related to their extended electrochemically active surface area (technological applications). However, only research activities conducted on basic (bulk-type) catalysts allow complete investigations of the reaction mechanisms (along with the individual stages), including important information on the catalyst's structural selectivity (see, e.g., refs. [29–31] for details).

As numerous organic molecules are susceptible to the catalytic surface electrosorption and reactivity phenomena, the presence of airborne organic compounds might have a significant impact on the performance of PEM fuel cells. Acetonitrile (AcN), with the chemical formula CH₃CN, is a highly polar and volatile organic solvent that is commonly used in various industrial applications, including extraction, plastic molding and casting, and some battery technologies. Therefore, its presence in the air can have a substantial (detrimental or positive) effect on the catalytic performance of noble metal-based electrochemical catalyst materials [32–37]. This work presents a comprehensive electrochemical study of the process of ethanol oxidation on a polycrystalline Pt electrode in 0.5 M H₂SO₄ and 0.1 M NaOH supporting solutions, examined comparatively in the absence and presence of acetonitrile, at the set AcN concentrations.

2. Results and Discussion

2.1. Electrooxidation of Ethanol by Cyclic Voltammetry in the Absence and Presence of Acetonitrile

The cyclic voltammetric behavior of the influence of acetonitrile on the process of ethanol electrooxidation (at 0.25 M C₂H₅OH) on a polycrystalline Pt electrode surface in 0.5 M H₂SO₄ and 0.1 M NaOH solutions is shown in Figure 1a–c below. For the experiments carried out in sulphuric acid supporting electrolyte, two oxidation peaks, centered at ca. 0.80 and 1.30 V vs. a reversible Pd hydrogen electrode (RHE), appear upon an anodic sweep (see the green plot in Figure 1a). Then, when the Cyclic Voltammetry (CV) sweep is reversed towards the hydrogen reversible potential, a single anodic peak, centered at about 0.60 V, appears in the CV profile. Ethanol electrooxidation follows a surface adsorption step of ethanol molecules, which most likely takes place over the potential range of ca. 0.20–0.40 V, partly in parallel with underpotentially deposited (UPD) H ionization from the Pt surface (see an inset to Figure 1a). The lowest potential oxidation peak (0.60 V) is typically assigned in the literature to the process of the oxidation of surface-adsorbed CO_{Ads} species, while that observed at 0.80 V is assigned to the formation of acetaldehyde [3,13,14,16]. On the contrary, the highest potential anodic peak, observed over the potential range of 1.10–1.50 V, corresponds to the oxidation process with the involvement of surface-adsorbed, oxygen-based species.

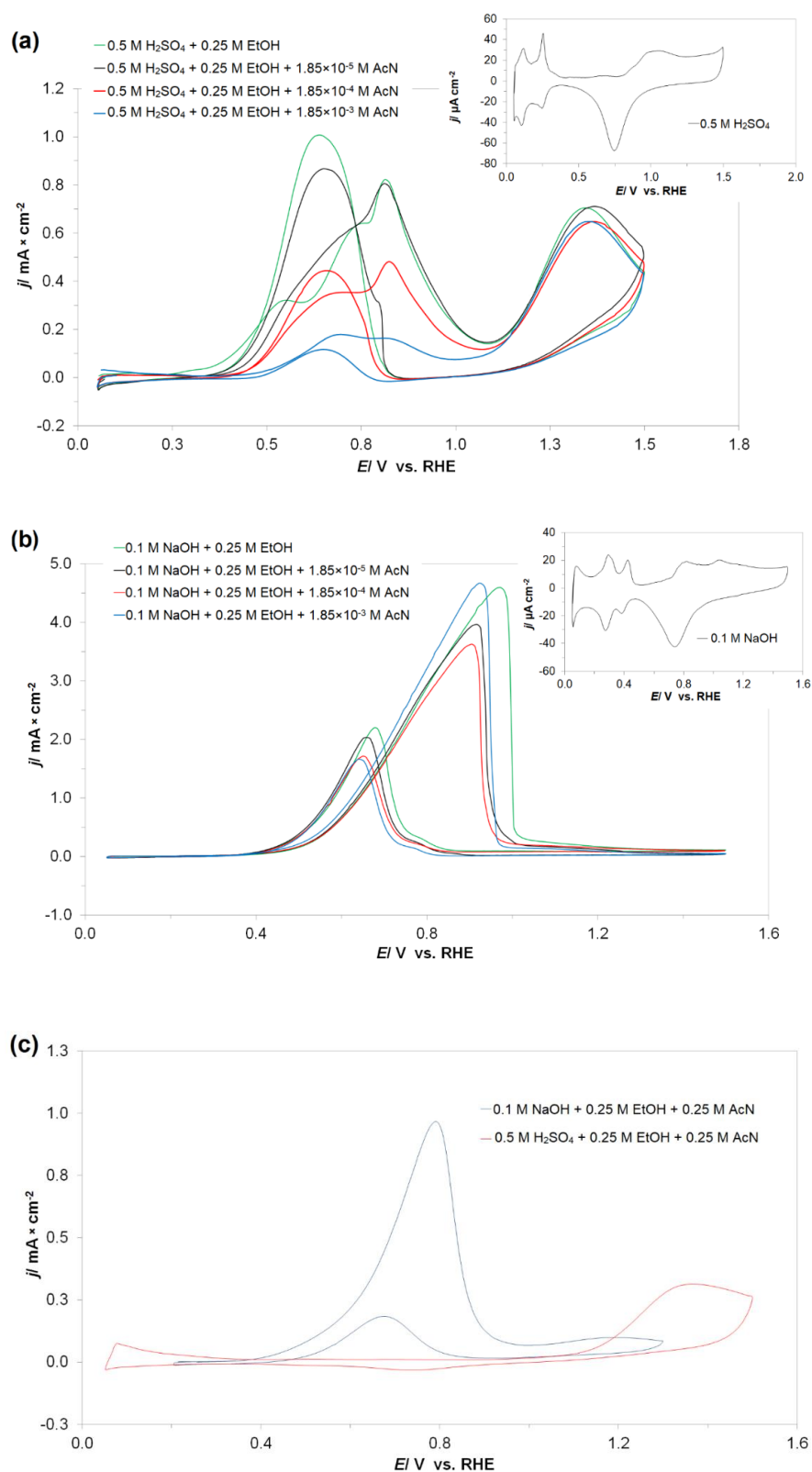
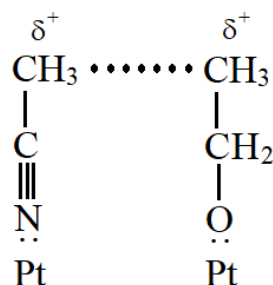


Figure 1. (a) Cyclic voltammograms for ethanol electrooxidation on a polycrystalline Pt electrode, carried out in 0.5 M H_2SO_4 and 0.25 M C_2H_5OH at a sweep rate of 50 mV s^{-1} , in the absence and presence of CH_3CN (at the concentrations indicated); the inset shows a cyclic voltammogram for a polycrystalline Pt electrode in pure 0.5 M H_2SO_4 ; (b) as in (a) above, but for 0.1 M NaOH supporting solution; (c) as in (a,b) above, but in the presence of 0.25 M CH_3CN .

Then, the introduction of acetonitrile into the electrolyte results in a successive, radical diminution of the maximum measured current-density and the voltammetric charge with respect to the 0.6 and 0.8 V oxidation processes (see the black, red, and blue plots in Figure 1a for the AcN concentrations of 1.85×10^{-5} , 1.85×10^{-4} , and 1.85×10^{-3} M, correspondingly). It is strongly believed that this phenomenon is associated with substantial inhibition of the Pt surface adsorption of C_2H_5OH molecules, due to extensive AcN co-adsorption, along with the repulsive interaction of such-formed entities on the surface of a polycrystalline platinum electrode (see a plausible model for the C_2H_5OH/CH_3CN Pt surface co-adsorptive interaction in Scheme 1 below).



Scheme 1. Chemisorption and mutual interaction of CH_3CN and C_2H_5OH molecules on the Pt surface.

On the other hand, Figure 1b presents the influence of acetonitrile on the process of C_2H_5OH electrooxidation on a poly Pt electrode, but examined in 0.1 M NaOH solution. Hence, a single oxidation peak, positioned at ca. 0.95 V vs. RHE (again, assigned to the formation of acetaldehyde), appears upon an anodic sweep. Then, when the cyclic voltammetry sweep is reversed towards the hydrogen reversible potential, another oxidation peak (centered at ca. 0.70 V: oxidation of surface-adsorbed CO_{Ads} species) arises in the CV profile (black plot in Figure 1b; also see the cyclic voltammetric profile of a poly Pt electrode in ethanol-free 0.1 M NaOH solution in an inset to this figure). Contrary to the behavior in sulphuric acid, the influence of AcN on the process of ethanol electrooxidation (apart from some shift of the peak potential points towards less positive potentials) is radically less evident in sodium hydroxide supporting electrolyte, even at the highest concentration of acetonitrile (compare the black plots with red, blue, and green plots in Figure 1b, respectively).

Interestingly, a significantly higher acetonitrile concentration (0.25 M AcN) was needed to cause a radical impediment (through Pt surface blockage) of the ethanol oxidation process in NaOH (Figure 1c). A key point in the observed difference for the EOR between H_2SO_4 (with almost complete surface blockage in the presence of 0.25 M AcN, observed over the potential range of 0.4–1.1 V) and NaOH supporting electrolytes is related to the concurrent adsorption of hydroxyl (OH^-) anions, which become electrosorbed in sodium hydroxide over the potential range characteristic of the process of ethanol oxidation. Surface-adsorbed OH species not only tend to stabilize (via dipole–dipole interactions) the Pt-adsorbed ethanol molecules, but also prevent the extensive adsorption of acetonitrile molecules. The latter is in line with the conclusions of recently published work from this laboratory (see Ref. [8,38] given there), where, contrary to the conditions encountered in sulphuric acid, acetonitrile adsorption in NaOH was practically limited to the potential range positive to that of UPD of H.

2.2. Influence of AcN on Ethanol Electrooxidation by a.c. Impedance Spectroscopy

The a.c. impedance behavior of the process of ethanol electrooxidation (in the absence and presence of CH_3CN) on the polycrystalline Pt electrode surface in 0.5 M H_2SO_4 and 0.1 M NaOH supporting solutions is presented in Tables 1 and 2, as well as Figure 2a–c (equivalent circuit models employed to fit the recorded impedance data), Figures 3a–c and 4a–c.

Table 1. Resistance and capacitance parameters for the electrooxidation of ethanol (at 0.25 M C₂H₅OH) on a polycrystalline Pt electrode in 0.5 M H₂SO₄ (at 293 K) in the absence and presence of acetonitrile (at four indicated acetonitrile (AcN) concentrations), obtained by finding the equivalent circuits which best fitted the impedance data, as shown in Figure 2a,b.

<i>E/mV</i>	<i>R_{ct}/Ω × cm²</i>	<i>C_{dl}/μF × cm⁻²</i>	<i>R_{Ads}/Ω × cm²</i>	<i>C_p/μF × cm⁻²</i>
0.5 M H ₂ SO ₄ + 0.25 M C ₂ H ₅ OH				
550	1524 ± 34	29.3 ± 0.9	-	-
650	2831 ± 243	53.2 ± 0.4	-3371 ± 263	69.1 ± 3.1
700	948 ± 60	37.9 ± 0.5	-1055 ± 37	97.0 ± 5.2
800	-439 ± 11	31.1 ± 0.5	-301 ± 1	60.2 ± 1.1
900	-1043 ± 83	36.9 ± 0.6	-854 ± 6	48.8 ± 0.6
0.5 M H ₂ SO ₄ + 0.25 M C ₂ H ₅ OH + 1.85 × 10 ⁻⁵ M AcN				
550	1587 ± 39	19.6 ± 0.4	-	-
650	3852 ± 505	42.6 ± 0.3	-7697 ± 387	61.1 ± 1.3
700	2294 ± 219	33.3 ± 0.4	-2188 ± 56	67.7 ± 1.6
800	-451 ± 17	22.9 ± 0.4	-442 ± 3	22.6 ± 0.6
900	-1408 ± 112	28.7 ± 0.4	-1021 ± 7	40.3 ± 0.8
0.5 M H ₂ SO ₄ + 0.25 M C ₂ H ₅ OH + 1.85 × 10 ⁻⁴ M AcN				
550	1330 ± 14	42.1 ± 0.5	-	-
650	3000 ± 131	54.6 ± 1.0	-	-
700	1664 ± 26	32.7 ± 0.5	-1000 ± 111	664.1 ± 46.7
800	-2506 ± 459	20.8 ± 0.4	-379 ± 4	108.2 ± 1.7
900	-784 ± 124	35.6 ± 0.5	-214 ± 4	254.7 ± 11.0
0.5 M H ₂ SO ₄ + 0.25 M C ₂ H ₅ OH + 1.85 × 10 ⁻³ M AcN				
550	2460 ± 61	71.6 ± 1.4	-	-
650	3028 ± 62	50.5 ± 0.4	-	-
700	4192 ± 167	37.7 ± 0.4	-12,716 ± 2406	101.4 ± 9.0
800	9168 ± 2328	17.2 ± 0.2	-20,223 ± 1957	27.8 ± 1.2
900	-5929 ± 1895	28.4 ± 0.7	-5936 ± 105	30.2 ± 0.5
0.5 M H ₂ SO ₄ + 0.25 M C ₂ H ₅ OH + 0.25 M AcN				
550	131,404 ± 11,769	57.9 ± 0.5	-	-
900	52,759 ± 3174	43.6 ± 0.8	-	-

Table 2. Resistance and capacitance (and inductance) parameters for the electrooxidation of ethanol (at 0.25 M C₂H₅OH) on a polycrystalline Pt electrode in 0.1 M NaOH (at 293 K), in the absence and presence of acetonitrile (at four indicated AcN concentrations), obtained by finding the equivalent circuits which best fitted the impedance data, as shown in Figure 2a,c.

<i>E/mV</i>	<i>R_{ct}/Ω × cm²</i>	<i>C_{dl}/μF × cm⁻²</i>	<i>R_O/Ω × cm²</i>	<i>L/H</i>
0.1 M NaOH + 0.25 M C ₂ H ₅ OH				
600	2211 ± 91	26.4 ± 1.1	604 ± 47	247 ± 10
675	2842 ± 257	27.5 ± 1.9	494 ± 38	155 ± 8
800	121 ± 1	69.3 ± 0.3	-	-
0.1 M NaOH + 0.25 M C ₂ H ₅ OH + 1.85 × 10 ⁻⁵ M AcN				
600	1648 ± 53	28.0 ± 1.2	713 ± 55	328 ± 16
675	1428 ± 102	30.4 ± 2.9	482 ± 100	264 ± 26
800	141 ± 1	81.4 ± 1.8	-	-
0.1 M NaOH + 0.25 M C ₂ H ₅ OH + 1.85 × 10 ⁻⁴ M AcN				
600	1558 ± 61	27.9 ± 1.4	1123 ± 95	315 ± 25
675	659 ± 18	26.6 ± 1.7	-	-
800	101 ± 1	85.0 ± 1.7	-	-

Table 2. Cont.

E/mV	$R_{ct}/\Omega \times cm^2$	$C_{dl}/\mu F \times cm^{-2}$	$R_O/\Omega \times cm^2$	L/H
0.1 M NaOH + 0.25 M C ₂ H ₅ OH + 1.85 × 10 ⁻³ M AcN				
600	598 ± 7	28.5 ± 0.9	805 ± 70	380 ± 22
675	215 ± 2	34.2 ± 1.2	-	-
800	61 ± 1	109.4 ± 5.4	-	-
0.1 M NaOH + 0.25 M C ₂ H ₅ OH + 0.25 M AcN				
600	1770 ± 13	19.0 ± 0.3	-	-
800	16,046 ± 461	24.3 ± 0.3	-	-

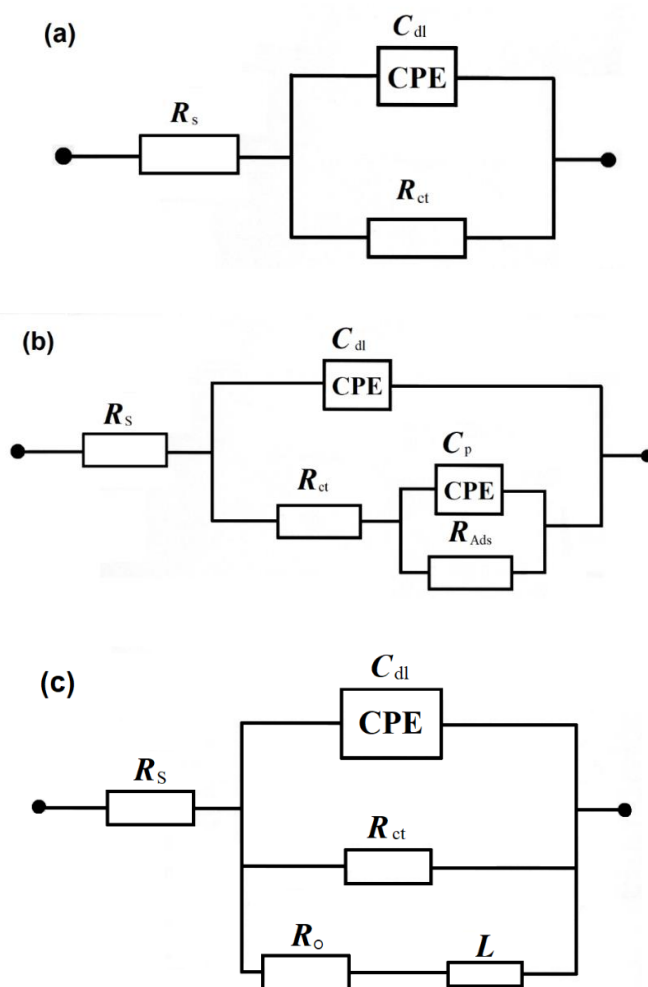


Figure 2. Three equivalent circuits (a–c), used for fitting the obtained a.c. impedance spectroscopy data in this work, where R_s is the solution resistance; C_{dl} is the double-layer capacitance; R_{ct} is the charge-transfer resistance parameter for the electrooxidation of ethanol; R_{Ads} and C_p are resistance and pseudocapacitance parameters for adsorbed reaction intermediates, respectively; and R_o and L are inductive resistance and inductance parameters, respectively. The circuits include constant phase elements (CPEs) to account for distributed capacitance.

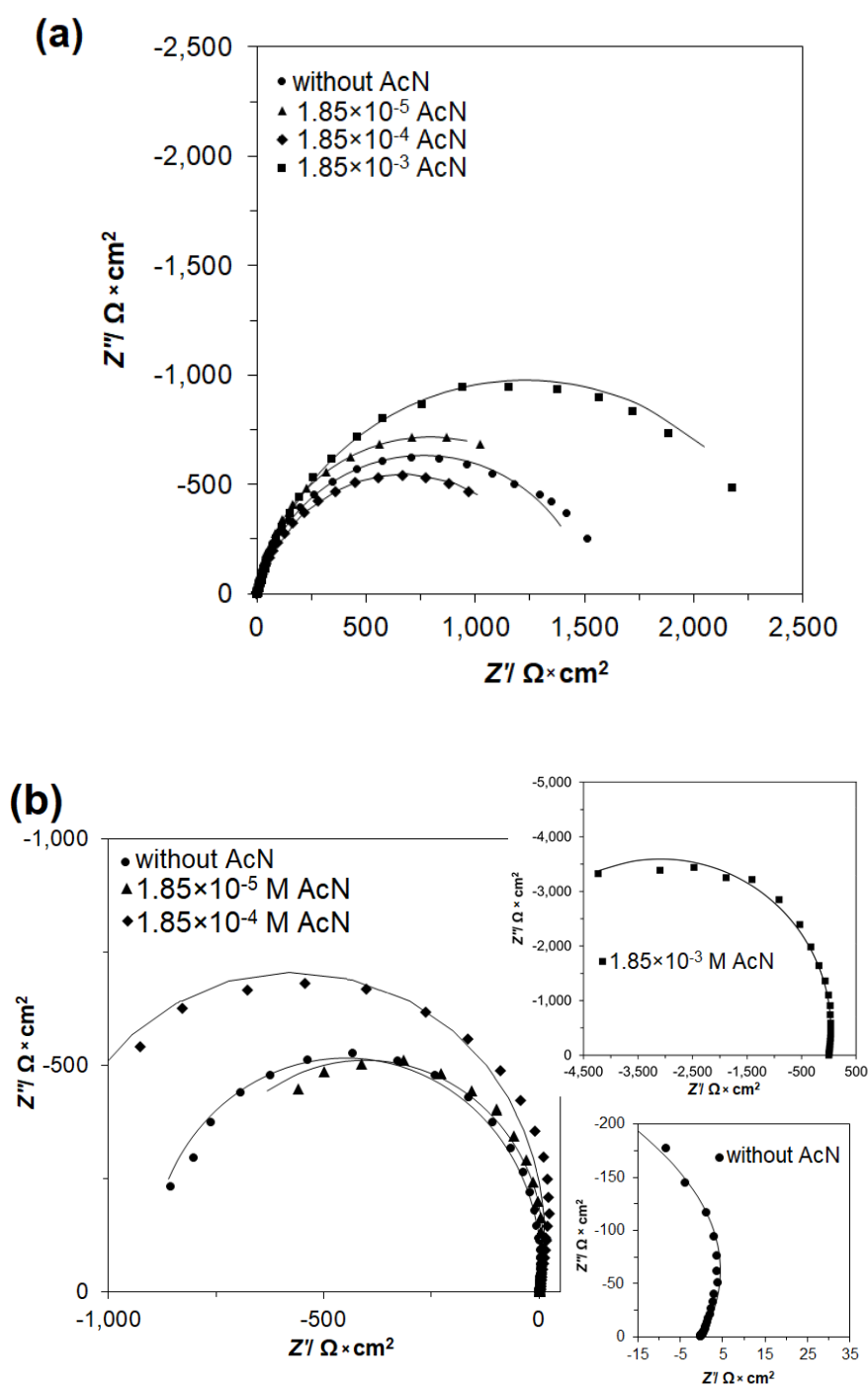


Figure 3. Cont.

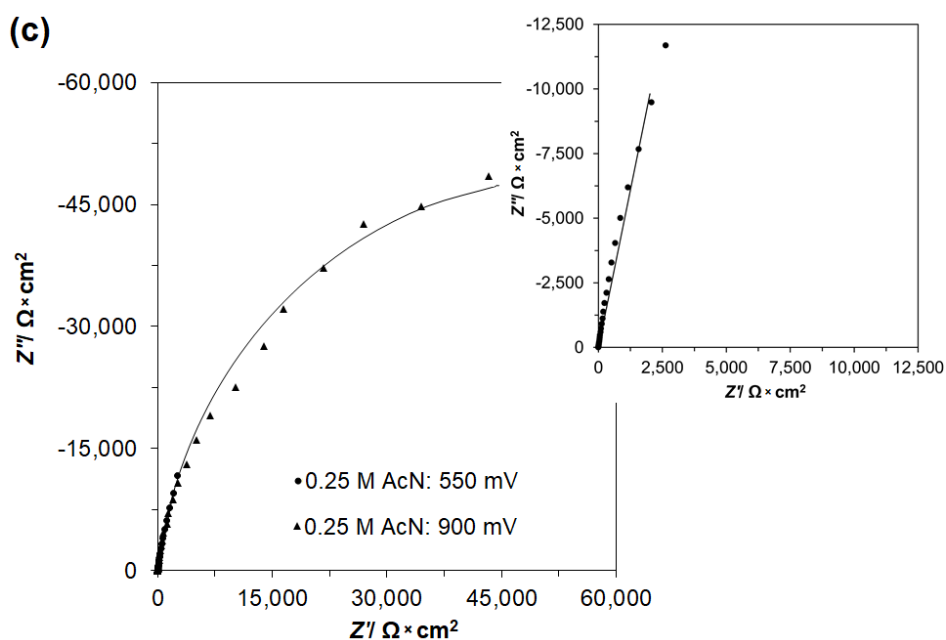


Figure 3. (a) Complex-plane impedance plot for a polycrystalline Pt electrode in contact with 0.5 M H_2SO_4 and 0.25 M $\text{C}_2\text{H}_5\text{OH}$, recorded at 550 mV vs. a reversible Pd hydrogen electrode (RHE) (at 293 K), in the absence and presence of CH_3CN (at the concentrations indicated). The solid lines correspond to representation of the data according to the equivalent circuit shown in Figure 2a; (b) as in (a) above, but for the potential of 900 mV (in reference to Figure 2b), where the inset shows an example of a high frequency semicircle response; (c) as in (a,b) above, but in the presence of 0.25 M CH_3CN .

A single partial semicircle (related to the process of ethanol electrooxidation in H_2SO_4) appears at the potential of 550 mV in the Nyquist impedance plot (see Figures 2a and 3a below). It should be noted, however, that a radical detrimental effect of acetonitrile on the recorded charge-transfer resistance R_{ct} parameter could only be observed for the two highest AcN concentrations of 1.85×10^{-3} and 0.25 M AcN. Here, the R_{ct} resistance values were 1524, 2460, and 131,404 $\Omega \times \text{cm}^2$ for AcN-free, 1.85×10^{-3} , and 0.25 M AcN (see Figure 3c) working in 0.5 M $\text{H}_2\text{SO}_4 + 0.25$ M $\text{C}_2\text{H}_5\text{OH}$ electrolyte, correspondingly. This behavior reflects a prevailing, acetonitrile Pt surface adsorption effect over that for ethanol molecules (also see Scheme 1 above), being simultaneously in line with the cyclic voltammetry features observed in Figure 1a. Then, for the potential ranges of 650–900 mV ($[\text{AcN}] = 0$ and 1.85×10^{-5} M) and 700–900 mV ($[\text{AcN}] = 1.85 \times 10^{-4}$ and 1.85×10^{-3} M), the impedance spectra are characterized by two partial semicircles (an inset to Figure 3b shows an example of a high frequency arc). Here, the high frequency semicircle response represents the reaction charge-transfer process (R_{ct}, C_{dl}), whereas a low frequency response would be associated with the surface adsorption of reaction intermediates (R_{Ads}, C_p). As can be seen in Table 1, all recorded R_{Ads} and also some high potential R_{ct} resistances exhibited negative values (also refer to the corresponding Nyquist plots with a negative real impedance part in Figure 3b). The above is indicative of instability within the examined electrochemical system, which most likely involves surface oscillation of the adsorbed reaction intermediates (also see Refs. [39–43] for details). Most importantly, increasing the AcN concentration (along with rising AcN platinum surface adsorption) generally caused augmentation of the R_{ct} and R_{Ads} resistance parameters (their absolute values), where simultaneously absolute values of the adsorption resistance parameter became considerably reduced upon a rising electrode potential (see Table 1 for details).

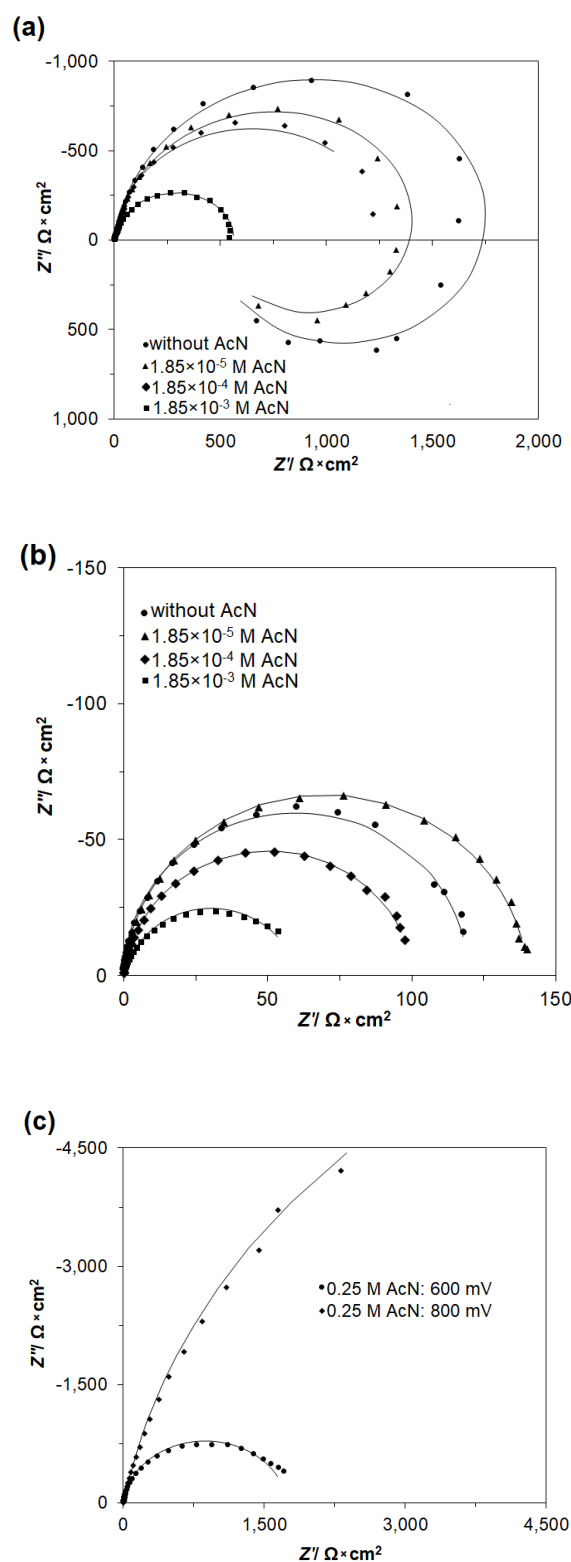
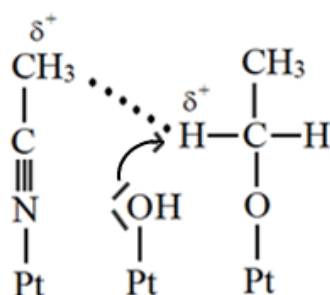


Figure 4. (a) Complex-plane impedance plot for a polycrystalline Pt electrode in contact with 0.1 M NaOH and 0.25 M $\text{C}_2\text{H}_5\text{OH}$, recorded at 600 mV vs. RHE (at 293 K), in the absence and presence of CH_3CN (at the concentrations indicated). The solid lines correspond to representation of the data according to the equivalent circuit shown in Figure 2c; (b) as in (a) above, but for the potential of 800 mV (in reference to Figure 2a); (c) as in (a,b) above, but in the presence of 0.25 M CH_3CN (in reference to Figure 2a).

On the other hand, the double-layer capacitance values C_{dl} showed significant fluctuations, from about 20 up to ca. $72 \mu\text{F} \times \text{cm}^{-2}$ (irrespective of the AcN concentration), where C_{dl} increased above the value of $20 \mu\text{F} \times \text{cm}^{-2}$ commonly used in the literature for smooth and homogeneous surfaces [44,45] could imply some contribution from the surface adsorption processes. At the same time, the pseudocapacitance C_p parameter exhibited reduction upon a rising electrode potential, e.g., from $69.1 \mu\text{F} \times \text{cm}^{-2}$ at 650 mV to $48.8 \mu\text{F} \times \text{cm}^{-2}$ at 900 mV vs. RHE for the AcN-free $\text{H}_2\text{SO}_4/\text{C}_2\text{H}_5\text{OH}$ solution. A deviation from the purely capacitive behavior required the use of the Constant Phase Element (CPE) components in the equivalent circuits (see Figure 2a,b). Here, this “capacitance dispersion” effect could be assigned to increasing Pt surface inhomogeneity, and a combination of repeatedly carried out flame-annealing procedures and extended potentiostatic impedance measurements [46–48]. In addition, the values of dimensionless φ_1 and φ_2 parameters for the CPE components oscillated between 0.62 and 0.94.

Furthermore, Table 2 and Figure 2a,c and Figure 4a–c present the a.c. impedance spectroscopy examination of the ethanol (again, at 0.25 M $\text{C}_2\text{H}_5\text{OH}$) electrooxidation reaction at the polycrystalline Pt electrode, but in 0.1 M NaOH supporting solution. In the absence of acetonitrile for the potentials of 600 and 675 mV (refer to the respective CV profile in Figure 1b), the corresponding Nyquist impedance spectra are characterized by a partial semicircle over the high frequency range and an inductive loop, exhibited over the low frequency end (Figure 4a). The presence of the inductive loop (also see the associated inductive resistance R_O and inductance L parameters in Table 2) is most likely related to the process of oxidative CO_{Ads} species removal from the Pt surface, thus leading to the release of platinum active sites [6,8]. Then, a single semicircle is present at 800 mV in the impedance spectrum, in relation to the surface formation of the acetaldehyde molecule (Figure 4b). The presence of CH_3CN in NaOH does not seem to have any detrimental effect on the process of $\text{C}_2\text{H}_5\text{OH}$ electrooxidation, until the AcN concentration exceeds the value of 1.85×10^{-3} M. On the contrary, the recorded charge-transfer resistance values seem to be inversely proportional to the rise in acetonitrile concentration (e.g., refer to a series of R_{ct} values, derived at 600 mV, of 2211, 1648, 1558, and $598 \Omega \times \text{cm}^2$, recorded for the CH_3CN concentrations of 0, 1.85×10^{-5} , 1.85×10^{-4} , and 1.85×10^{-3} M, respectively).

Therefore, it could be concluded that CH_3CN (except for the highest 0.25 M concentration) was found to cause significant facilitation of the EOR in NaOH supporting solution, which the authors believe could be due to additional $[\text{CH}_3 \cdots \text{H}]$ interactions (facilitating alcohol dehydrogenation) between the surface-adsorbed species, as illustrated in Scheme 2 below. This finding could additionally be supported by a radical difference in the recorded voltammetric current-densities between acidic and alkaline supporting electrolytes, as shown in Figure 1a,b, correspondingly. In addition, as argued by Briega-Martos et al. in Ref. [49] (on the role of acetonitrile in electrocatalytic enhancement of the HCOOH oxidation reaction), the fact that relatively low acetonitrile concentrations lead to EOR facilitation might also result from the so-called CH_3CN “promoting effect”, due to its ability to block Pt sites from the extended formation of CO_{Ads} species or through stabilizing dipole–dipole interactions with the surface-adsorbed reaction intermediates, e.g., acetaldehyde.



Scheme 2. Chemisorption and mutual interactions of CH_3CN and $\text{C}_2\text{H}_5\text{OH}$ molecules on the Pt surface in NaOH supporting solution.

In fact, in the presence of 0.25 M AcN, the R_{ct} resistance becomes radically increased (especially at the potential of 800 mV to over $16.000 \Omega \times \text{cm}^2$, see Figure 4c). These findings are totally in line with those previously documented (for 0.1 M NaOH solution) by the cyclic voltammetry behavior in Figure 1b,c, where the recorded maximum voltammetric current-density in Figure 1c (0.25 M CH_3CN) only reached about 20% of that recorded in the presence of 1.85×10^{-3} M AcN. Moreover, the C_{dl} parameter exhibited similar fluctuation (ca. $19\text{--}109 \mu\text{F} \times \text{cm}^{-2}$) to that observed for sulphuric acid supporting solution presented in Table 1, whereas the values of dimensionless parameters φ_3 and φ_4 oscillated between 0.87 and 0.99. Deterioration of the EOR kinetics at a very high concentration of acetonitrile is undoubtedly a result of very limited $\text{C}_2\text{H}_5\text{OH}$ adsorption, due to the prevalent Pt surface co-adsorption of CH_3CN molecules.

2.3. Spectrophotometric UV-VIS Analysis of Ethanol Oxidation Products

The assessment of acetaldehyde and acetate contents was performed by means of the UV-VIS spectrophotometry technique. The derived concentration values of ethanol oxidation by-products were in fairly good agreement with the results of the electrochemical measurements for both supporting solutions.

Increased CH_3CN concentrations in the H_2SO_4 -based solution resulted in a significant reduction of the EOR by-products' generation rate. After 3 min of continuous electrooxidation, the concentration of acetaldehyde reached ca. 0.12, 0.04, and 0.03 M for the following solutions: AcN-free, 1.85×10^{-5} , and 0.25 M CH_3CN , correspondingly. Analogous behavior was observed for the recorded acetate concentrations of about 0.10, 0.02, and 0.02 M for the baseline solutions of AcN-free, 1.85×10^{-3} , and 0.25 M CH_3CN , respectively. Then, after the initial three minutes of the process, the current-density became significantly impeded for all examined sulfuric acid-based experimental samples, resulting in no noticeable differences between the by-product concentrations in the further ongoing EOR process. The above was most likely caused by the poisoning effect of the Pt electrochemically active surface by the reaction products, mainly the CO_{Ads} species.

Figure 5a,b below present the changes of CH_3CHO and CH_3COO^- concentrations, recorded as the time of the ethanol electrooxidation process in 0.1 M NaOH-based solution, respectively. Here, the reaction time (up to 30 min), along with initial AcN content, had practically no influence on the resulting concentrations of the products. The catalytic decomposition of ethanol (under the influence of acetonitrile upon solution electrolysis) led (primarily) to the formation of acetaldehyde and acetic acid (or rather acetate ions) molecules. The observed fluctuation of the recorded concentrations of acetaldehyde and acetate over the duration of electrolysis resulted from the fact that both CH_3CHO and CH_3COO^- species are characterized by a high water solubility and volatility (high vapor pressure), in addition to their well-known surface adsorption properties. In other words, during the course of the experiment, one should expect equilibrated concentration (with some fluctuation) behavior of the product, rather than its continuous increase, which is totally in line with the findings of Figure 5.

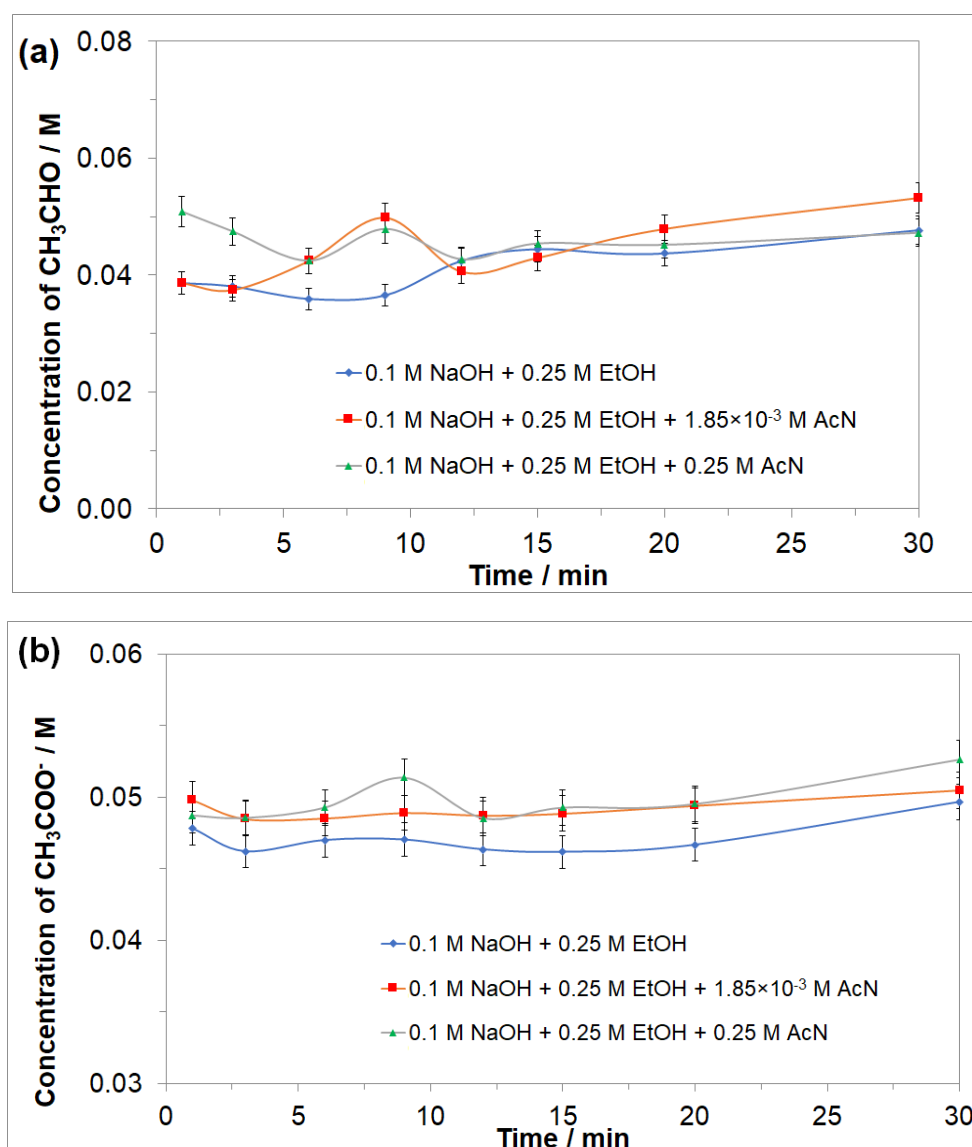


Figure 5. Representation of acetaldehyde (a) and acetate (b) concentrations recorded during the initial 30 min of ethanol electrooxidation, carried out in 0.1 M NaOH supporting electrolyte.

3. Materials and Methods

3.1. Solutions and Solutes

High-purity electrolytes were made from water derived from an 18.2 MΩ Direct-Q3 UV ultra-pure water purification system from Millipore-Merck (Burlington, MA, USA). Aqueous, 0.5 M H₂SO₄, and 0.1 M NaOH solutions were prepared from sulphuric acid of the highest purity available (SEASTAR Chemicals, Sidney, BC, Canada) and AESAR, 99.996% sodium hydroxide pellets, correspondingly. Ethanol (POCH, pure, p.a., Gliwice, Poland) was used to prepare acidic and alkaline solutions at concentrations of 0.25 M C₂H₅OH. In addition, acetonitrile (electronic grade, 99.999% trace metals basis, Sigma-Aldrich (Saint Louis, MO, USA)) was introduced to the solutions by means of Eppendorf micro-pipettes to obtain AcN concentrations of 1.85×10^{-5} , 1.85×10^{-4} , 1.85×10^{-3} , and 0.25 M. Before conducting the experiments, all solutions were de-aerated with high-purity argon (Ar 6.0 grade, Linde (Kraków, Poland)), whose flow was maintained above the solutions' mirror during all electrochemical experiments.

3.2. Electrochemical Cell and Electrodes

An electrochemical cell, made of Pyrex glass, was used during the course of this work. The cell comprised three electrodes: A polycrystalline Pt (1 mm diameter 99.9985% Pt wire: AESAR/Puratronic, $S_A = 0.64 \text{ cm}^2$) working electrode (WE) in a central part; a reversible Pd hydrogen electrode (RHE; coiled 0.5 mm diameter, 99.9% purity Pd wire, Sigma-Aldrich (Saint Louis, MO, USA), sealed in soft glass) as a reference; and a Pt counter electrode (CE; coiled 1.0 mm diameter, 99.9998% purity Pt wire, Johnson Matthey, Inc. (London, UK), also sealed in soft glass), in separate cell sections. Before its use, the Pd RHE was cleaned in hot sulphuric acid, followed by cathodic charging with hydrogen in 0.5 M H_2SO_4 (at a current of $I_C = 20 \text{ mA}$), until large quantities of H_2 bubbles in the electrolyte were distinctly observed. Both the working and counter electrodes, prior to their use, were flame-annealed and quenched with ultra-pure water.

In order to minimize the ohmic resistance (IR) drop, the Luggin capillary was placed at the center of the cell (also, a 0.5 mm diameter Pt wire was inserted between and within the tip of the Luggin capillary and the RHE reference compartment). Prior to each series of experiments, the electrochemical cell was taken apart and soaked in hot sulphuric acid for 3 h. After cooling down to ca. 30–35 °C, the cell (along with all of its components) was carefully rinsed with Millipore ultra-pure water.

3.3. Electrochemical and other Equipment

Cyclic voltammograms were recorded at room temperature (296 K), at a sweep rate of 50 mV s^{-1} , by means of the Solartron 12,608 W Full Electrochemical System (1260 frequency response analyzer–FRA + 1287 electrochemical interface (EI)) (Solartron Group, Farnborough, UK). For a.c. impedance measurements, the 1260 FRA generator provided an output signal of a 5 mV amplitude and the frequency range was kept between 1.0×10^5 and $0.5 \times 10^{-1} \text{ Hz}$. The instruments were controlled by ZPlot 2.9 or Corrware 2.9 software for Windows (Scribner Associates, Inc., Southern Pines, NC, USA). The impedance results presented in this work were obtained through the selection and analysis of representative data series, where two to three impedance measurements were carried out at each potential value. The reproducibility of such-recorded results was below 10% from one measurement to another. The impedance data analysis was performed with the ZView 2.9 (Scribner Associates, Inc., Southern Pines, NC, USA) software package, where the spectra were fitted by means of a complex, non-linear, least-squares immitance fitting program—LEVM 6—written by Macdonald [50]. Two equivalent circuits for identified charge-transfer surface processes, including constant-phase elements (CPEs) to account for distributed capacitance, were employed to analyze the obtained impedance results, as shown in Figure 2a–c in the Results and Discussion section.

3.4. Assessment of Acetaldehyde and Acetate Contents upon Progress of the Ethanol Electrooxidation Reaction

Ethanol electrooxidation trials (at 0.25 M $\text{C}_2\text{H}_5\text{OH}$) were performed for both H_2SO_4 and NaOH supporting solutions over the period of 30 min for the following AcN concentrations: 0, 1.85×10^{-3} , and 0.25 M CH_3CN . The trials involved continuous CV cycling (at the sweep rate of 50 mV s^{-1}) over the working electrode potential range of 0.4–1.0 V/RHE.

In order to evaluate the content of acetaldehyde, the reaction of aldehydes with a Schiff's reagent (commercial reagent, Chempur, Piekary Śląskie, Poland) was used. The collected samples (acidic ones after alkalization to a pH of about 9.0) were initially mixed with Schiff's reagent at a 1:2 volume ratio and incubated for 10 min at room temperature. On the contrary, a color reaction with iron III chloride was used to determine the concentration of acetate ions in working electrolyte samples. For this purpose, the samples were mixed with 0.1 M $\text{FeCl}_3 \times 6\text{H}_2\text{O}$ solution (POCH, Gliwice, Poland) again at a 1:2 volume ratio, and incubated for 10 min at room temperature. Then, absorbance values were derived through spectrophotometric measurements, carried out at wavelengths of $\lambda = 550 \text{ nm}$ (acetaldehyde samples) and $\lambda = 450 \text{ nm}$ (acetate specimens) by means of an EPOCH 2 plate reader (BioTek, Winooski, VT, USA). The obtained results were then compared with the standard curves.

4. Conclusions

The ethanol oxidation reaction (EOR) gains its technological importance through the application of ethanol solution in direct ethanol fuel cell devices. A combination of a.c. impedance spectroscopy and cyclic voltammetry electrochemical techniques, and spectrophotometric UV-VIS analysis (necessary to assess the efficiency of key reaction products), allowed us to effectively examine the influence of acetonitrile (an important industrial solvent and possible environmental contaminant) on the kinetics of the ethanol electrooxidation reaction, performed on a polycrystalline platinum electrode surface.

The obtained results provided evidence for a significant and damaging role of Pt surface-adsorbed acetonitrile in the process of ethanol oxidation in sulphuric acid solution. On the contrary, under alkaline experimental conditions, adsorbed CH₃CN molecules (at relatively low concentrations) could function as the reaction-promoting element through mutual dipole–dipole stabilizing interactions, which, except for acetonitrile, also include hydroxyl OH species and surface-adsorbed reaction intermediates. In the latter case, the EOR becomes radically facilitated, which implies the significant importance of alkaline-based DAFC technologies, under frequently encountered environmental (industrial) conditions.

Author Contributions: Conceptualization, B.P.; methodology, B.P.; investigation, M.L., T.M., and P.W.; data curation, T.M. and M.L.; writing—original draft preparation, B.P.; editing, B.P. and T.M.; supervision, L.S. All authors have read and agreed to the published version of the manuscript.

Funding: Project financially supported by the Minister of Science and Higher Education in the range of the program entitled “Regional Initiative of Excellence” for the years 2019–2022, Project No. 010/RID/2018/19, amount of funding 12,000,000 PLN.

Acknowledgments: This work has been financed by the internal research grant no. 20.610.001-300, provided by The University of Warmia and Mazury in Olsztyn. Mateusz Luba would also like to acknowledge a scholarship from the program Interdisciplinary Doctoral Studies in Bioeconomy (POWR.03.02.00-00-1034/16-00), funded by the European Social Fund.

Conflicts of Interest: The authors declare no conflict of interest.

References

1. Rousseau, C.; Countaneceau, C.; Lamy, C.; Leger, J.M. Direct ethanol fuel cell (DEFC): Electrical performances and reaction products distribution under operating conditions with different platinum-based anodes. *J. Power Sources* **2006**, *158*, 18–24. [[CrossRef](#)]
2. Song, S.Q.; Zhou, W.J.; Zhou, Z.H.; Jiang, L.H.; Sun, G.Q.; Xin, Q.; Leontidis, V.; Kontou, S.; Tsiakaras, P. Direct ethanol PEM fuel cells: The case of platinum based anodes. *Int. J. Hydrog. Energy* **2005**, *30*, 995–1001. [[CrossRef](#)]
3. Abd-El-Latif, A.A.; Mostafa, E.; Huxter, S.; Attard, G.; Baltrischat, H. Electrooxidation of ethanol at polycrystalline and platinum stepped single crystals: A study by differential electrochemical mass spectrometry. *Electrochim. Acta* **2010**, *55*, 7951–7960. [[CrossRef](#)]
4. Han, S.B.; Song, Y.J.; Lee, J.M.; Kim, J.Y.; Park, K.W. Platinum nanocube catalysts for methanol and ethanol electrooxidation. *Electrochem. Commun.* **2008**, *10*, 1044–1047. [[CrossRef](#)]
5. Shao, M.H.; Adzic, R.R. Electrooxidation of ethanol on a Pt electrode in acid solutions: In situ ATR-SEIRAS study. *Electrochim. Acta* **2005**, *50*, 2415–2422. [[CrossRef](#)]
6. Gupta, S.S.; Singh, S.; Datta, J. Temperature effect on the electrode kinetics of ethanol electro-oxidation on Sn modified Pt catalyst through voltammetry and impedance spectroscopy. *Mater. Chem. Phys.* **2010**, *120*, 682–690. [[CrossRef](#)]
7. Switzer, E.E.; Olson, T.S.; Datye, A.K.; Atanassov, P.; Hibbs, M.R.; Cornelius, C.J. Templated Pt–Sn electrocatalysts for ethanol, methanol and CO oxidation in alkaline media. *Electrochim. Acta* **2009**, *54*, 989–995. [[CrossRef](#)]
8. Mahapatra, S.S.; Dutta, A.; Datta, J. Temperature effect on the electrode kinetics of ethanol oxidation on Pd modified Pt electrodes and the estimation of intermediates formed in alkali medium. *Electrochim. Acta* **2010**, *55*, 9097–9104. [[CrossRef](#)]

9. Hassan, K.M.; Hathoot, A.A.; Maher, R.; Azzem, M.A. Electrocatalytic oxidation of ethanol at Pd, Pt, Pd/Pt and Pt/Pd nano particles supported on poly 1,8-diaminonaphthalene film in alkaline medium. *RSC Adv.* **2018**, *8*, 15417–15426. [[CrossRef](#)]
10. Abdel, R.M.H. Nickel Oxide Nanoparticles Supported on Graphitized Carbon for Ethanol Oxidation in NaOH Solution. *J. Clust. Sci.* **2019**, *30*, 1003–1016. [[CrossRef](#)]
11. Monyoncho, E.A.; Woo, T.K.; Baranova, E.A. Ethanol electrooxidation reaction in alkaline media for direct ethanol fuel cells. In *SPR-Electrochemistry*; Banks, C., McIntosh, S., Eds.; Royal Society of Chemistry: London, UK, 2019; Volume 15, pp. 1–57.
12. Gupta, S.S.; Datta, J. A Comparative Study on Ethanol Oxidation Behavior at Pt and PtRh Electrodeposits. *J. Electroanal. Chem.* **2006**, *594*, 65–72. [[CrossRef](#)]
13. Xia, X.H.; Liess, H.D.; Iwasita, T. Early stages in the oxidation of ethanol at low index single crystal platinum electrodes. *J. Electroanal. Chem.* **1997**, *437*, 233–240. [[CrossRef](#)]
14. Gomes, J.F.; Busson, B.; Tadjeddine, A.; Tremiliosi-Filho, G. Ethanol electro-oxidation over Pt(h k l): Comparative study on the reaction intermediates probed by FTIR and SFG spectroscopies. *Electrochim. Acta* **2008**, *53*, 6899–6905. [[CrossRef](#)]
15. El-Shafei, A.A.; Eiswirth, M. Electrochemical activity of Sn-modified Pt single crystal electrodes for ethanol oxidation. *Surf. Sci.* **2010**, *604*, 862–867. [[CrossRef](#)]
16. Pierozynski, B. Kinetic Aspects of Ethanol Electrooxidation on Catalytic Surfaces of Pt in 0.5 M H₂SO₄. *Int. J. Electrochem. Sci.* **2012**, *7*, 3327–3338.
17. Pierozynski, B. On the Ethanol Electrooxidation Reaction on Catalytic Surfaces of Pt in 0.1 M NaOH. *Int. J. Electrochem. Sci.* **2012**, *7*, 4261–4271.
18. Fujiwara, N.; Siroma, Z.; Yamazaki, S.; Ioroi, T.; Senoh, H.; Yasuda, K. Direct ethanol fuel cells using an ion exchange membrane. *J. Power Sources* **2008**, *185*, 621–626. [[CrossRef](#)]
19. Pierozynski, B. Electrooxidation of Ethanol on PtRh and PtRu Surfaces Studied in 0.5 M H₂SO₄: Relation to the Behaviour at Polycrystalline Pt. *Int. J. Electrochem. Sci.* **2012**, *7*, 4488–4497.
20. Pierozynski, B. Ethanol Electrooxidation on PtRh and PtRu Catalytic Surfaces in 0.1 M NaOH. *Int. J. Electrochem. Sci.* **2012**, *7*, 6406–6416.
21. Simoes, F.C.; dos Ainos, D.M.; Vigier, F.; Leger, J.M.; Hahn, F.; Coutanceau, C.; Gonzalez, E.R.; Tremiliosi-Filho, G.; de Andrade, A.R.; Olivi, P.; et al. Electroactivity of tin modified platinum electrodes for ethanol electrooxidation. *J. Power Sources* **2007**, *167*, 1–10. [[CrossRef](#)]
22. Luo, Z.; Lu, J.; Flox, C.; Nafria, R.; Genc, A.; Arbiol, J.; Llorca, J.; Ibanez, M.; Morante, J.R.; Cabot, A. Pd₂Sn [010] nanorods as a highly active and stable ethanol oxidation catalyst. *J. Mater. Chem. A* **2016**, *4*, 16706–16713. [[CrossRef](#)]
23. Guo, J.; Chen, R.; Zhu, F.-C.; Sun, S.-G.; Villullas, H.M. New understanding of ethanol oxidation reaction mechanism on Pd/C and Pd₂Ru/C catalysts in alkaline direct ethanol fuel cells. *Appl. Catal. B Environ.* **2018**, *224*, 602–611. [[CrossRef](#)]
24. Delpeuch, A.B.; Maillard, F.; Chatenet, M.; Soudant, P.; Cremers, C. Ethanol oxidation reaction (EOR) investigation on Pt/C, Rh/C, and Pt-based bi- and tri-metallic electrocatalysts: A DEMS and in situ FTIR study. *Appl. Catal. B Environ.* **2015**, *181*, 672–680. [[CrossRef](#)]
25. Yi, J.; Lee, W.H.; Choi, C.H.; Lee, Y.; Park, K.S.; Min, B.K.; Hwang, Y.J.; Oh, H.-S. Effect of Pt introduced on Ru-based electrocatalyst for oxygen evolution activity and stability. *Electrochem. Commun.* **2019**, *104*, 1–5. [[CrossRef](#)]
26. Su, C.; Yang, T.; Zhou, W.; Wang, W.; Xu, X.; Shao, Z. Pt/C-LiCoO₂ composites with ultralow Pt loadings as synergistic bifunctional electrocatalysts for oxygen reduction and evolution reaction. *J. Mater. Chem. A* **2016**, *4*, 4516–4524. [[CrossRef](#)]
27. Sasaki, K.; Marinkovic, N.; Isaacs, H.S.; Adzic, R.R. Synchrotron-Based in situ characterization of Carbon-supported platinum and platinum monolayer electrocatalysts. *ACS Catal.* **2016**, *6*, 69–76. [[CrossRef](#)]
28. Da Silva, G.C.; Fernandes, M.R.; Ticianelli, E.A. Activity and Stability of Pt/IrO₂ Bifunctional Materials as Catalysts for the Oxygen Evolution/Reduction Reactions. *ACS Catal.* **2018**, *8*, 2081–2092. [[CrossRef](#)]
29. Pierozynski, B.; Morin, S.; Conway, B.E. Influence of adsorption of guanidonium cations on H upd at Pt(hkl) surfaces: Lattice-specific anion-mimetic effects. *J. Electroanal. Chem.* **1999**, *467*, 30–42. [[CrossRef](#)]
30. Wang, Y.; Zou, S.; Cai, W.B. Recent advances on electro-oxidation of ethanol on Pt- and Pd-based catalysts: From reaction mechanisms to catalytic materials. *Catalysts* **2015**, *5*, 1507–1534. [[CrossRef](#)]

31. Hitmi, H.; Belgsir, E.; Léger, J.-M.; Lamy, C.; Lezna, R. A kinetic analysis of the electro-oxidation of ethanol at a platinum electrode in acid medium. *Electrochim. Acta* **1994**, *39*, 407–415. [[CrossRef](#)]
32. Reshетенко, T.V.; St-Pierre, J. Study of the acetonitrile poisoning of platinum cathodes on proton exchange membrane fuel cell spatial performance using a segmented cell system. *J. Power Sources* **2015**, *293*, 929–940. [[CrossRef](#)]
33. Briega-Martos, V.; Costa-Figueiredo, M.; Orts, J.M.; Rodes, A.; Koper, M.T.M.; Herrero, E.; Feliu, J.M. Acetonitrile adsorption on Pt single-crystal electrodes and its effect on oxygen reduction reaction in acidic and alkaline aqueous solutions. *J. Phys. Chem. C* **2019**, *123*, 2300–2313. [[CrossRef](#)]
34. Ahlberg, E.; Friel, M. The cathodic polarization of iron in acidic acetonitrile-water solutions. *Electrochim. Acta* **1989**, *34*, 771–780. [[CrossRef](#)]
35. Ledezma-Yanez, I.; Diaz-Morales, O.; Figueiredo, M.C.; Koper, M.T.M. Hydrogen oxidation and hydrogen evolution on a platinum electrode in acetonitrile. *ChemElectroChem* **2015**, *2*, 1612–1622. [[CrossRef](#)]
36. Smiljanić, M.L.; Srejić, I.L.; Marinović, V.M.; Rakočević, Z.L.; Štrbac, S.B. Inhibiting effect of acetonitrile on oxygen reduction on polycrystalline Pt electrode in sodium chloride solution. *Hem. Ind.* **2012**, *66*, 327–333. [[CrossRef](#)]
37. Srejić, I.; Smiljanić, M.; Rakočević, Z.; Štrbac, S. Oxygen reduction on polycrystalline Pt and Au electrodes in perchloric acid solution in the presence of acetonitrile. *Int. J. Electrochem. Sci.* **2011**, *6*, 3344–3354.
38. Mikolajczyk, T.; Luba, M.; Pierozynski, B.; Smoczynski, L. A detrimental effect of acetonitrile on the kinetics of underpotentially deposited hydrogen and hydrogen evolution reaction, examined on Pt electrode in H₂SO₄ and NaOH solutions. *Catalysts* **2020**, *10*, 625. [[CrossRef](#)]
39. Ma, B.; Dong, L. Electrochemical impedance analysis of methanol oxidation on carbon nanotube-supported Pt and Pt-Ru nanoparticles. *J. Solid State Electrochem.* **2013**, *17*, 2783–2788. [[CrossRef](#)]
40. Danaee, I.; Jafarian, M.; Forouzandeh, F.; Gobal, F.; Mahjani, M.G. Electrochemical impedance studies of methanol oxidation on GC/Ni and GC/NiCu electrode. *Int. J. Hydrog. Energy* **2009**, *34*, 859–869. [[CrossRef](#)]
41. Bommersbach, P.; Mohamedi, M.; Guay, D. Electro-oxidation of Ethanol at Sputter-Deposited Platinum-Tin Catalysts. *J. Electrochem. Soc.* **2007**, *154*, B876–B882. [[CrossRef](#)]
42. Benetton, X.D.; Navarro-Avila, S.G.; Carrera-Figueiras, C. Electrochemical Evaluation of Ti/TiO₂-polyaniline Anodes for Microbial Fuel Cells using Hypersaline Microbial Consortia for Synthetic-wastewater Treatment. *J. New Mater. Electrochem. Syst.* **2010**, *13*, 1–6.
43. Han, L.; Ju, H.; Xu, Y. Ethanol electro-oxidation: Cyclic voltammetry, electrochemical impedance spectroscopy and galvanostatic oscillation. *Int. J. Hydrog. Energy* **2012**, *37*, 15156–15163. [[CrossRef](#)]
44. Lasia, A.; Rami, A. Kinetics of hydrogen evolution on Ni-Al alloy electrodes. *J. Appl. Electrochem.* **1992**, *22*, 376–382.
45. Chen, L.; Lasia, A. Study of the Kinetics of Hydrogen Evolution Reaction on Nickel-Zinc Alloy Electrodes. *J. Electrochem. Soc.* **1991**, *138*, 3321–3328. [[CrossRef](#)]
46. Pajkossy, T. Impedance of rough capacitive electrodes. *J. Electroanal. Chem.* **1994**, *364*, 111–125. [[CrossRef](#)]
47. Conway, B.E. *Impedance Spectroscopy: Theory, Experiment, and Applications*; Barsoukov, E., Macdonald, J.R., Eds.; Wiley: Hoboken, NJ, USA, 2005; p. 494.
48. Pell, W.G.; Zolfaghari, A.; Conway, B.E. Capacitance of the double-layer at polycrystalline Pt electrodes bearing a surface-oxide film. *J. Electroanal. Chem.* **2002**, *532*, 13–23. [[CrossRef](#)]
49. Briega-Martos, V.; Solla-Gullon, J.; Koper, M.T.M.; Herrero, E. Electrocatalytic enhancement of formic acid oxidation reaction by acetonitrile on well-defined platinum surfaces. *Electrochim. Acta* **2019**, *295*, 835–845. [[CrossRef](#)]
50. Macdonald, J.R. *Impedance Spectroscopy: Emphasizing Solid Materials and Systems*; Wiley: New York, NY, USA, 1987.

Publisher's Note: MDPI stays neutral with regard to jurisdictional claims in published maps and institutional affiliations.



© 2020 by the authors. Licensee MDPI, Basel, Switzerland. This article is an open access article distributed under the terms and conditions of the Creative Commons Attribution (CC BY) license (<http://creativecommons.org/licenses/by/4.0/>).